Acta Materialia 166 (2019) 47–55

Contents lists available at ScienceDirect

Acta Materialia

journal homepage: www.elsevier.com/locate/actamat

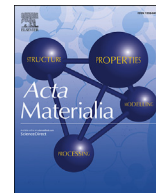

Full length article

Identification of the nature of traps involved in the field cycling of $Hf_{0.5}Zr_{0.5}O_2$-based ferroelectric thin films

Damir R. Islamov [a, b, *], Vladimir A. Gritsenko [a, b, c], Timofey V. Perevalov [a, b], Vladimir A. Pustovarov [d], Oleg M. Orlov [e], Anna G. Chernikova [f], Andrey M. Markeev [f], Stefan Slesazeck [g], Uwe Schroeder [g], Thomas Mikolajick [g, h], Gennadiy Ya Krasnikov [e]

[a] Rzhanov Institute of Semiconductor Physics, Siberian Branch of the Russian Academy of Sciences, 13 Lavrentiev Avenue, Novosibirsk, 630090, Russian Federation
[b] Novosibirsk State University, 2 Pirogov Street, Novosibirsk, 630090, Russian Federation
[c] Novosibirsk State Technical University, 20 Karl Marx Avenue, Novosibirsk, 630073, Russian Federation
[d] Experimental Physics Department, Ural Federal University, 19 Mira Street, Yekaterinburg, 620002, Russian Federation
[e] Molecular Electronic Research Institute, 12/1 1-st Zapadniy Proezd, Zelenograd, Moscow, 124460, Russian Federation
[f] Moscow Institute of Physics and Technology (State University), 9 Institutsky Pereulok, Dolgoprudny, 141700, Moscow region, Russian Federation
[g] NaMLab gGmbH, 64 Noethnitzer Strasse, Dresden, 01187, Germany
[h] Institute of Semiconductors and Microsystems, TU Dresden, 10 Helmholtzstraße, Dresden, 01062, Germany

ARTICLE INFO

Article history:
Received 13 July 2018
Received in revised form
4 December 2018
Accepted 7 December 2018
Available online 11 December 2018

Keywords:
Ferroelectric $Hf_{0.5}Zr_{0.5}O_2$
Defects
Luminescence
Oxygen vacancies
Leakage currents

ABSTRACT

The discovery of ferroelectricity in hafnium oxide has revived the interest in ferroelectric memories as a viable option for low power non-volatile memories. However, due to the high coercive field of ferroelectric hafnium oxide, instabilities in the field cycling process are commonly observed and explained by the defect movement, defect generation and field induced phase transitions. In this work, the optical and transport experiments are combined with *ab-initio* simulations and transport modeling to validate that the defects which act as charge traps in ferroelectric active layers are oxygen vacancies. A new oxygen vacancy generation leads to a fast growth of leakage currents and a consequent degradation of the ferroelectric response in $Hf_{0.5}Zr_{0.5}O_2$ films. Two possible pathways of the $Hf_{0.5}Zr_{0.5}O_2$ ferroelectric property degradation are discussed.

© 2018 Acta Materialia Inc. Published by Elsevier Ltd. All rights reserved.

1. Introduction

Semiconductor memories are an important ingredient in today's and future electronic systems. The trend of having electronics integrated into almost every object called Internet of Things will require to have a non-volatile memory in nearly every device. Additionally, in today's computing systems, both energy efficiency and performance are strongly limited by the memory access via the so called von Neumann bottleneck. Moreover, DRAM memories have almost reached its scaling limit and traditional floating gate-based memory cells are becoming very difficult and therefore expensive to be integrated in 28 nm CMOS processes and beyond. Consequently, the pull for introducing new memory concepts has strongly intensified for the last decade. Different types of memories are used in state of the art computing systems. The processing unit needs to access the code and some data in a random fashion. This is currently realized by SRAM and DRAM memories. The former have a very large area and, therefore, cost much, while the later have reached their scaling limits. Therefore, an alternative technology for both of them is highly desirable. On the other end of the hierarchy are the storage devices currently realized by the NAND Flash. These are now fabricated in the 3D technology stacking as many as 96 cells on top of each other and storing up to 4 bits in every cell. Since the random access speed of these type of memories is of a very slow (in the 100 μs) range, there is a huge gap in the random access speed between the RAM and the storage device. The storage class memory having a specification in-between RAM and NAND Flash has, therefore, become an important object of research and development. Besides the standalone memories mentioned before,

* Corresponding author. Rzhanov Institute of Semiconductor Physics, Siberian Branch of the Russian Academy of Sciences, 13 Lavrentiev Avenue, Novosibirsk, 630090, Russian Federation.
E-mail address: damir@isp.nsc.ru (D.R. Islamov).

https://doi.org/10.1016/j.actamat.2018.12.008
1359-6454/© 2018 Acta Materialia Inc. Published by Elsevier Ltd. All rights reserved.

the demand for having embedded non-volatile memories in CMOS processes is growing rapidly since mobile devices always need a certain amount of local memory. In this arena different flavors of NOR Flash memories based on a floating gate or the charge trapping technology have been used down to the 40 nm node. However, for 28 nm and beyond, the high-κ metal gate, FD-SOI, FinFET and other innovations are introduced, the integration challenge of these devices is drastically increasing, and simpler solutions are highly desirable. To fulfill the demands described above, several approaches to alternative memories have been intensively researched for the last 20 years. The most important are, e.g., Phase Change Memory, Magnetoresistive Random Access Memory, Resistive Random Access Memory (RRAM) and Ferroelectric Memories (FRAM).

In this paper we will focus on an important issue of ferroelectric memories. The first 1T-1C based conventional FRAM devices were commercialized in as early as 1990 [1]. However, due to the complications of integrating a complex oxide, like lead zirconium titanate (PZT) or strontium-bismuth tantalate (SBT), in a CMOS process [2], the scaling was much slower compared to competing technologies and it completely stopped at the point where a 3D capacitor would have to be introduced to get enough charge out of the ferroelectric switching for a reliable sensing [3]. In 2011, a ferroelectric effect in doped hafnium oxide films of a thickness ~6–10 nm was reported for the first time. Since hafnium oxide is a material already integrated in sub 40 nm CMOS technologies, this event has resumed the interest in ferroelectric memories as a promising memory technology [4–6]. The easiest way to stabilize the ferroelectric phase in HfO_2 requires doping with various elements, like Si, Al, Y, Gd, La and others, followed by high-temperature annealing ($\sim$ 1000 °C). Of particular interest is the fact that ferroelectric properties have also been demonstrated in the thin solid solution $Hf_{0.5}Zr_{0.5}O_2$ films, for which the required annealing temperature is relatively low [6–10]. This makes this material compatible with the back-end of the line process. The ferroelectric effect in hafnia-based materials is associated with the possibility of stabilizing the nonequilibrium noncentral-symmetric orthorhombic phase $Pbc2_1$ in them [6,11]. Different flavors of implementation ranging from 1T FeFET [12] over 1T1C FRAM [13] up to 1T1R concepts relying on ferroelectric tunnel junctions [11] are under intensive research.

Using doped hafnium oxide, currently, an endurance of about 10^{10} cycles has been reported on the capacitor level [14]. Since the RAM type of memories would require unlimited endurance, much work has been put into understanding and optimizing the endurance on the material level [15–17]. It is well understood that the generation and redistribution of defects in the hafnium oxide has a strong contribution to this degradation [15,16]. The defects are speculated to be related to oxygen vacancies. However, no clear evidence for this speculation could be given yet. The purpose of this study is to close this gap by identifying the transport mechanisms, as well as to determine the nature (atomic and electronic structure) of the traps responsible for the charge transport in orthorhombic ferroelectric $Hf_{0.5}Zr_{0.5}O_2$, and, therefore, to come one step closer to clarifying their role in the field cycling.

2. Experimental methods

2.1. Preparation of test structures

Metal-insulator-metal TiN/$Hf_{0.5}Zr_{0.5}O_2$ /TiN and TiN/$Hf_{0.5}Zr_{0.5}O_2$ /Pt structures were prepared for optical and transport experiments. A 15-nm-thick TiN layer was deposited on the oxidized Si (100) substrate using the atomic layer deposition (ALD) technique. Then the $Hf_{0.5}Zr_{0.5}O_2$ films were deposited at 240 °C from TEMAH and TEMAZ precursors using H_2O as an oxygen source. The TEMAH and TEMAZ precursors were mixed in a single-cocktail balloon before the ALD process. After that the samples were annealed at 400 °C in the N_2 environment for 30 s by rapid thermal annealing (RTA). Laser ellipsometry and Rutherford backscattering spectroscopy confirmed the thickness d and the stoichiometry of deposited $Hf_{0.5}Zr_{0.5}O_2$ films. The crystalline structures of annealed films were examined by symmetrical X-Ray diffraction using the ARL X'TRA tool (Thermo Scientific) utilizing the Cu$K\alpha$ radiation.

The endurance and transport measurements were performed for the test structures with the 10-nm-thick $Hf_{0.5}Zr_{0.5}O_2$ film. On the 10-nm-thick $Hf_{0.5}Zr_{0.5}O_2$ films the TiN top layer (10-nm-thick) was deposited using the ALD technique. For the transport measurements, round (area $= 7.854 \times 10^3\ \mu m^2$) electrodes were formed by a photolithography process.

'Thick' 20-nm $Hf_{0.5}Zr_{0.5}O_2$ films were fabricated for optical experiments. On the 'thick' ($d = 20$ nm) $Hf_{0.5}Zr_{0.5}O_2$ films a 30-nm-thick Pt top layer was deposited by the electron beam evaporation through a shadow mask. The Pt contacts were used for the $Hf_{0.5}Zr_{0.5}O_2$ film ferroelectric property confirmation only. The optical measurements were carried out on the $Hf_{0.5}Zr_{0.5}O_2$ surface between Pt plaques.

The contact to bottom TiN electrode was made by the Ar^+ ion etching.

2.2. Characterization of test structures

The presence of $Hf_{0.5}Zr_{0.5}O_2$ film ferroelectric properties is confirmed by observing the hysteresis in the polarization-voltage characteristics for TiN/$Hf_{0.5}Zr_{0.5}O_2$ /Pt (See Supplementary Fig. S1) and TiN/$Hf_{0.5}Zr_{0.5}O_2$ /TiN (Fig. 1(b)) structures. To provide a wake-up of ferroelectric response in thick $Hf_{0.5}Zr_{0.5}O_2$ (20 nm) films, 10 consecutive switching patterns are required. The presence of hysteresis indicates that the ferroelectric phase is also present in the 'thick' films. It should be noted that the photoluminescence signal of the 10-nm-thick films is very week and cannot be separated from noise even at LN_2 temperatures. That is why we used 20-nm-thick samples for the optical measurements to investigate the electronic structures of the defects in HfO_2-based materials.

2.3. Ferroelectric switch cycling

The set/reset cycling (endurance) measurements were performed by the successive pulses of the applied voltage ± 2.5 V to avoid early breakdown. The pulse increase/decrease duration was 8 ns, the pulse shelf duration was 5 μs. The gap between pulses was 5 μs to avoid local heating during cycling and to prevent structure puncturing by probe needles due to thermal expansion. The total write/erase cycle time of $\approx 20\ \mu$s accords to the frequency of 50 kHz. In the Supplementary Fig. S2(a) the pulse forms and characteristics are represented in detail.

2.4. Polarization- and current-voltage measurements

Instead of some set/reset cycles (see supplementary S2 section), the polarization-voltage (P-V) and current-voltage (I-V) dependencies were measured by the modified PUND (Positive-Up-Negative-Down) technique at room temperature using a voltage sweep of about 0.05 Hz by an Agilent B1500A Semiconductor Device Parameter Analyzer. The first 'P' and the third 'N' triangle impulses aligned the dipoles in the ferroelectric films (set and reset, respectively), and they were used in measuring polarization, while, during the second 'U' and the forth 'D' impulses, the leakage currents were measured. The pulse amplitude was 2.5 V, the sweep step was 0.05 V with the duration of 5.4 μs, 1000 measurements

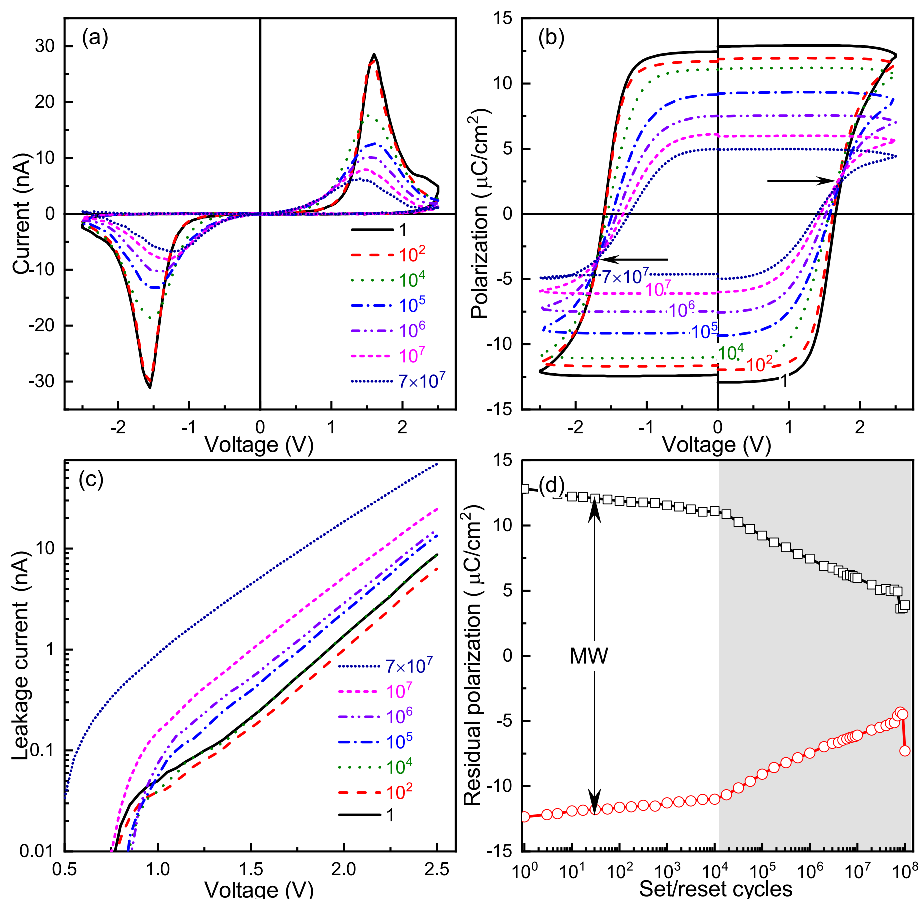

Fig. 1. Evolution of the TiN/$Hf_{0.5}Zr_{0.5}O_2$ (10 nm)/TiN transport and ferroelectric properties during the set/reset cycling (endurance). (a) Current-voltage characteristics in the 'P' and 'N' parts of 'PUND' measurements. (b) Polarization-voltage hysteresis. The cross-points are shown with arrows. (c) The leakage current-voltage dependencies extracted from the 'U' and 'D' parts of 'PUND' measurements. (d) Evolution of the residual polarization and memory window.

were made during one triangle pulse (totally, 4000 measurements were made during the full PUND cycle for 21.6 s). In the Supplementary Fig. S2(b), the pulse forms and characteristics are shown in detail.

The leakage currents were extracted from the current responses by removing the displacement currents by averaging the forward ($0 \to \pm V$) and reverse ($\pm V \to 0$) strokes of the voltage sweep:

$$I^{U}_{\text{leakage}}(V) = \frac{1}{2}\left(I^{U}_{0\to +V}(V) + I^{U}_{+V\to 0}(V)\right),$$

$$I^{D}_{\text{leakage}}(V) = \frac{1}{2}\left(I^{D}_{0\to -V}(V) + I^{D}_{-V\to 0}(V)\right).$$

Supplementary Fig. S3 schematically represents this procedure. The control DC measurements demonstrated that the leakage currents did not depend on the sweep rate in the used range.

2.5. Optical measurements

The DDS400 deuterium lamp and the primary double-prism monochromator DMR-4 were used for the photoluminescence (PL) excitation. The PL spectra were recorded using a secondary DMR-4 double-prism monochromator and a Hamamatsu R6358-10 type photomultiplier tube. The PL excitation (PLE) spectra were normalized to the equal number of photons incident on the sample using a yellow lumogen — a luminophore with the known energy quantum yield over the studied spectral range. The PL emission spectra were not corrected for the spectral sensitivity of the registration system.

The cathodoluminescence (CL) spectra were studied at the electron energy of 2 keV (penetration depth is 80 nm) and the current of 10 nA.

2.6. Ab-initio simulations

The electronic structure of oxygen vacancy in orthorhombic o-$Hf_{0.5}Zr_{0.5}O_2$ was investigated within the spin polarized density functional theory (DFT) using the *ab initio* simulation code Quantum ESPRESSO with the B3LYP hybrid exchange-correlation functional [18,19]. The oxygen vacancy was generated by the removal of an O atom, followed by the relaxation of all remaining atoms in a 96-atom supercell. The structure was obtained by replacing half of the Hf atom by Zr in the orthorhombic HfO_2 cell [20]. The atom selection for the replacement was carried out on the minimal total energy basis. Three oxygen vacancy types of were investigated: one with the fourfold (2 Hf and 2 Zr, named 'HHZZ') and two with the threefold coordination (2 Hf and 1 Zr, named 'HHZ', as well as 1 Hf and 2 Zr, named 'HZZ'). The Bloch functions of electrons in the crystal were represented by the plane-wave expansions with the cutoff energy of 55 Ry. The atomic arrangement was optimized with the force convergence threshold of 0.04 eV/Å performed within the standard DFT.

The optical properties of $Hf_{0.5}Zr_{0.5}O_2$ were calculated at a random phase approximation for the cubic phase. The choice of the

cubic phase is justified according to the simplicity of its structure and of the corresponding computational efforts. For the simulation, 96-atom c-$Hf_{0.5}Zr_{0.5}O_2$ supercells were used.

The thermal and optical trap ionization energy values were calculated using the approach described in Ref. [21]:

$$E^q_{\rm opt} = E^{q+1}_{{\rm d}(q)} - E^q_{{\rm d}(q)} + E^{-1}_{\rm p} - E^0_{\rm p}, \quad (1)$$

$$E^q_{\rm th} = E^q_{\rm opt} - E^q_{\rm relax} = E^q_{\rm opt} - \left[E^q_{{\rm d}(q-1)} - E^q_{{\rm d}(q)}\right]. \quad (2)$$

Here $E_{\rm p}{}^0$ and $E_{\rm p}{}^{-1}$ are the total energies of a neutral and negatively charged (with one additional electron) defect-free supercell. $E^q_{{\rm d}(q)}$ is the total energy of the supercell with an oxygen vacancy with charge $q = -2, -1, 0$ and $+1$ with relaxed geometry; $E^{q+1}_{{\rm d}(q)}$ is the total energy of the supercell with the oxygen vacancy with charge $(q+1)$, but with the geometry corresponding to a vacancy with charge q. $E^q_{\rm relax}$ is the relaxation energy of the supercell with the oxygen vacancy with charge q.

3. Theory

3.1. Extracting the trap density from leakage currents

The trap density was extracted from the *I-V* dependencies of the leakage currents within a model of phonon-assisted tunneling between traps (PATT). Recently, it has been demonstrated, that this transport model adequately describes the leakages in both amorphous and ferroelectric $Hf_{0.5}Zr_{0.5}O_2$ [22,23]. For the first time, the multiphonon-assisted trap ionization model was proposed by Makram-Ebeid and Lannoo [24]. This model described the charge transport in excellent agreement with the experimental data in case of isolated traps in dielectrics. So, the distance between neighbor traps is long enough to suppress the charge-carrier hoppings between traps [25,26]. In case of close neighbor traps, an additional transport channel, due to quantum tunneling effects, should be taken into account [27]. In the stationary case with an arbitrary trap distribution, the transport equation can be written as in Ref. [28].

$$a\nabla\left(n_{\rm t}\left(1-\frac{n_{\rm t}}{N}\right)P\right) = \frac{1}{e}\nabla J, \quad (3)$$

where a is the (local) distance between neighbor traps, ∇ is the del operator representing the divergence here, $n_{\rm t}$ is the local charged trap density, N is the local total trap density, e is the elementary charge, J is the current density, P is the rate of the tunnel junction between neighboring traps proposed by Nasyrov and Gritsenko [27]:

$$P = \int\limits_{\varepsilon>0} \frac{\hbar\varepsilon}{m^* a^2 kTQ_0}\exp\left(-\frac{(Q-Q_0)^2-(Q-eFa/Q_0)^2}{2kT} - \frac{4}{3}\frac{\sqrt{2m^*}\left(\varepsilon^{3/2}-(\varepsilon-eFa)^{3/2}\right)}{eF\hbar}\right)dQ$$

$$\varepsilon = Q_0(Q-Q_0)+W_{\rm opt}, \quad Q_0 = \sqrt{2(W_{\rm opt}-W_{\rm t})}, \quad (4)$$

where $\hbar$ is the Planck constant, m^* is the charge carrier (electron or hole) effective mass, k is the Boltzmann constant, T is temperature, Q is the configuration coordinate of a trapped-electron-with-phonons system, F is the local electric field. The Lorenz corrections for polarized dielectrics $P_{\rm r}/3\varepsilon_0$ are not used because this term does not change the electron potential energy difference between neighboring traps eFa. Here and below, $P_{\rm r}$ is the residual polarization, ε_0 is the electric constant. Therefore, to simplify the calculations, we considered the field as $F = V/d$. Here '$-\varepsilon$' represents the energy (below conduction band bottom $E_{\rm c}$) of trapped electron interacted with phonons, and Q_0 is the configuration coordinate characterizing the electron-phonon interaction.

In case of uniform trap distribution $N = a^{-3}$, Eq. (3) can be solved as

$$J = \frac{e}{a^2}\frac{n_{\rm t}}{N}\left(1-\frac{n_{\rm t}}{N}\right)P, \quad (5)$$

where a^2 has the dimension of a trap cross-section, $n_{\rm t}/N$ represents a part of filled traps and $(1-n_{\rm t}/N)$ is the part of empty traps.

In case of low electric fields $eFa \ll W_{\rm t}$, Eq. (4) can be simplified to

$$P = \frac{2\sqrt{\pi}\hbar W_{\rm t}}{m^* a^2 Q_0\sqrt{kT}}\exp\left(-\frac{W_{\rm opt}-W_{\rm t}}{2kT}\right)\times\exp\left(-\frac{2a\sqrt{2m^*W_{\rm t}}}{\hbar}\right)\sinh\left(\frac{eFa}{2kT}\right). \quad (6)$$

Here, the pre-exponential factor is the attempt-to-escape frequency, the first exponent represents the thermal ionization with the activation energy of $(W_{\rm opt}-W_{\rm t})/2$, the next exponent is the tunneling factor and the last term indicates the activation energy decreasing due to the external electric field. Using Eqs. (5) and (6) one can extract the largest distance between neighboring traps from the slope of experimentally measured currents in the log(*J*)-vs-*F* plate.

The analysis shows that, in moderate and strong electric fields ($eFa \geqslant \frac{1}{4}W_{\rm t}$), Eq. (6) gives a significant deviation, and Eq. (4) should be used. In this case, the slope of *J-F* curves in the semilog plot corresponds to the largest distance between neighboring traps. The *I-V* plot can be converted to the *J-F* one for the analysis by dividing *I* by the sample area and *V* by the film thickness.

4. Results and discussion

4.1. General analysis

The evolution of transport and ferroelectric properties measured for TiN/$Hf_{0.5}Zr_{0.5}O_2$ (10 nm)/TiN structures during the set/reset cycling (endurance) is shown in Fig. 1. The pristine and stressed films exhibit a single peak in the current-voltage characteristics (see Fig. 1(a)) in the 'P' and 'N' parts of 'PUND' measurements and a hysteresis loop in the polarization–voltage plate (see Fig. 1(b)). It is interesting to note that all hysteresis exhibit two cross-points (arrows in Fig. 1(b)), where the polarization at a specific voltage (and electric field) does not depend on set/reset cycles. The same phenomenon was observed, but not discussed, in ferroelectric HfO_2:Si [29]. The nature of this effect requires a special research and is still under investigation.

The leakage currents extracted from 'U' and 'D' parts of 'PUND' measurements exhibit their exponential dependence on the applied voltage, as shown in Fig. 1(c). The leakage currents slightly decrease during 10^0–10^4 set/reset cycles, but they increase dramatically after 10^4 of the cycles. This increase correlates with the decrease of the memory window (MW), which is a difference between positive and negative residual polarities $\mathrm{MW} = \left|P^+_{\rm r}\right| + \left|P^-_{\rm r}\right|$ (see Fig. 1(d)). Before 10^4 cycles, in the operation mode, MW is reduced by no more than 3% per decade. After 10^4 cycles, in the fatigue mode, the MW reduction is about 20%/decade. Similar results were reported for ferroelectric HfO_2:Sr [15,30], Gd:HfO_2 [17], Y:HfO_2 [31,32]. Therein, they were interpreted as a

defects redistribution in the wake-up phase and the generation of additional defects leading to a leakage current increase in the fatigue phase. However, the underlying defects nature was not identified in Ref. [15].

4.2. Defect nature identification by optical methods

The photoluminescence spectrum of the 'thick' ferroelectric f-$Hf_{0.5}Zr_{0.5}O_2$ film under the 5.2 eV ultraviolet excitation is shown in Fig. 2(a). The dominant blue luminescence peak with the maximum at 2.7 eV is observed. In the photoluminescence excitation spectrum of the band with the energy of 2.7 eV, the maxima are observed at the energies of 3.7 eV, 4.5 eV and 5.2 eV (arrows in Fig. 2(b)). In the cathodoluminescence spectrum, the peak at 2.6 eV is observed, as shown in Fig. 2(c).

The calculated optical absorption spectrum of the oxygen vacancies of different configurations in $Hf_{0.5}Zr_{0.5}O_2$ exhibits its maximum at the energy of 5.1 eV (Fig. 2(d)). The position of the theoretically calculated optical absorption maximum of 5.1 eV is in a good agreement with the position of the experimentally determined 5.2 eV PLE peak in ferroelectric $Hf_{0.5}Zr_{0.5}O_2$ films. This result indicates that the peak with the energy of 5.2 eV in the excitation spectrum of the blue 2.7 eV luminescence band f-$Hf_{0.5}Zr_{0.5}O_2$ is due to the oxygen vacancy. The photons with the energy of 5.2 eV excite a blue luminescence band with the energy of 2.7 eV. Therefore, the blue luminescence in f-$Hf_{0.5}Zr_{0.5}O_2$ is due to the optical transitions in oxygen vacancies.

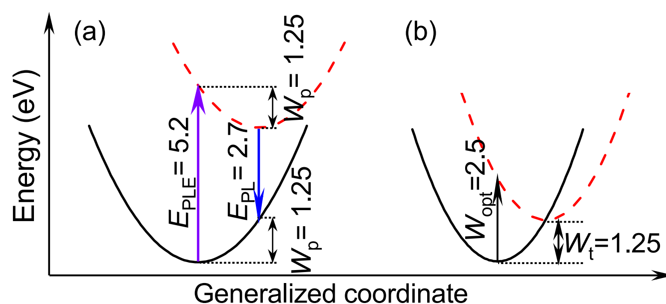

Fig. 3. Configuration coordination energy diagrams: (a) transitions on the neutral oxygen vacancy in $Hf_{0.5}Zr_{0.5}O_2$, (b) trap ionization on the negatively charged oxygen vacancy in $Hf_{0.5}Zr_{0.5}O_2$.

The empirical configuration diagram of optical transitions to the oxygen vacancies in f-$Hf_{0.5}Zr_{0.5}O_2$ is shown in Fig. 3(a). The lower term corresponds to the ground occupied state. The upper term corresponds to an empty excited state. The vertical transition with the energy of 5.2 eV corresponds to the luminescence excitation. The vertical transition with the energy of 2.7 eV corresponds to the radiative transition, blue luminescence. The polaron energy is equal to half of the Stokes shift of the luminescence due to oxygen vacancy $W_p = (5.2 - 2.7)/2 = 1.25$ eV. The polaron energy coincides with the thermal energy $W_p = W_t = 1.25$ eV for the trap which is responsible for the charge transport in $Hf_{0.5}Zr_{0.5}O_2$. Consequently,

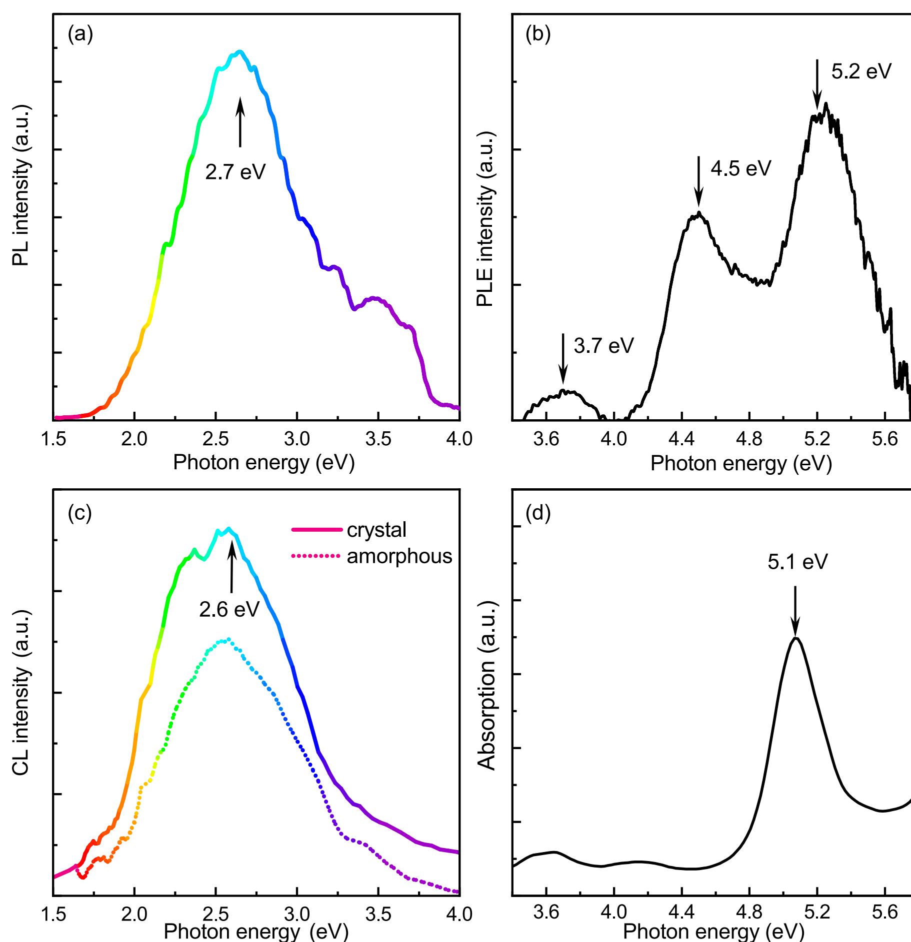

Fig. 2. $Hf_{0.5}Zr_{0.5}O_2$ spectra: (a) photoluminescence spectrum of f-$Hf_{0.5}Zr_{0.5}O_2$ under excitation 5.2 eV, (b) excitation spectrum of 2.7 eV photoluminescence band, (c) cathodoluminescence spectra of amorphous and ferroelectric $Hf_{0.5}Zr_{0.5}O_2$, (d) simulated optical absorption spectrum for the oxygen vacancy in f-$Hf_{0.5}Zr_{0.5}O_2$.

oxygen vacancies can act as traps responsible for the charge transport in $Hf_{0.5}Zr_{0.5}O_2$. The charge transport in $Hf_{0.5}Zr_{0.5}O_2$ is discussed below.

The general empirical configuration diagram of electronic transitions on a negatively charged trap (detrapping) in $Hf_{0.5}Zr_{0.5}O_2$ is shown in Fig. 3(b). The lower term corresponds to the ground occupied state. The upper term corresponds to the empty excited state. The vertical transition from the minimum of the ground state corresponds to optical trap energy W_{opt} . The difference between the minima of the ground and excited states corresponds to thermal trap energy W_t . To provide equality $W_{opt} = 2W_t$, the parabolas intersect at the minimum of the excited state.

The thermal and optical trap energies equality in the ferroelectric f-$Hf_{0.5}Zr_{0.5}O_2$ film, corresponding to the values obtained for the amorphous a-$Hf_{0.5}Zr_{0.5}O_2$ films, indicates the traps related nature in different phases [22,23]. Moreover, the obtained trap energy parameter values coincide with the corresponding parameters of a-$Hf_xZr_{1-x}O_y$ films synthesized by other methods (for example, by physical vapor deposition with the target heating by an electron beam) [22]. The identical nature of the traps in f-$Hf_{0.5}Zr_{0.5}O_2$ and a-$Hf_{0.5}Zr_{0.5}O_2$, also indicates the coincidence of the cathodoluminescence maximum energy of these films in Fig. 2(c).

4.3. Defect nature identification by ab-initio simulations

The position of the defect levels (Kohn-Sham single-electron states) related to the edges of the conduction and valence bands in a neutral, single and double negatively and positively charged oxygen vacancy with a different coordination in $Pbc2_1$ o-$Hf_{0.5}Zr_{0.5}O_2$ is shown in Fig. 4. With the addition of one/two electrons in the bandgap, a second localized single-filled/double-filled state is formed approximately 1 eV below E_c . A positively single-charged oxygen vacancy also forms an additional (unfilled) state below the conduction band bottom. The oxygen vacancy in o-$Hf_{0.5}Zr_{0.5}O_2$ charged by one electron, as well as by one hole, is a magnetic defect, which is indicated by the splitting of the completely filled lower level into two spin states. A double positively and negatively charged vacancy in o-$Hf_{0.5}Zr_{0.5}O_2$ is a nonmagnetic defect. A vacancy with two holes gives one empty state in the bandgap. With two additional electrons the oxygen vacancy gives two filled states in the bandgap.

The presented data indicate that the oxygen vacancy in o-$Hf_{0.5}Zr_{0.5}O_2$ can act as a localization center for both electrons and holes. This is confirmed by the estimates of the trap thermal and optical ionization energy values calculated using equations (1) and (2). The positive E_{opt} values shown in Table 1 indicate that the capture of both electron and hole on any type of oxygen vacancies in o-$Hf_{0.5}Zr_{0.5}O_2$ is energetically favorable. Thus, the oxygen vacancy in o-$Hf_{0.5}Zr_{0.5}O_2$ is an amphoteric defect for the charge localization. In other words, it can act as an electron and hole trap and participate in the charge transport.

Table 1
Optical E_{opt} and thermal E_{th} trap ionization energy values for the oxygen vacancy in o-$Hf_{0.5}Zr_{0.5}O_2$ in the coordination of HHZZ, HHZ and HZZ and in different charge states q calculated using Eqs. (1) and (2).

	Coord.	$q = -2$	$q = -1$	$q = 0$	$q = +1$
E_{opt} (eV)	HHZZ	0.46	0.69	2.46	2.75
	HHZ	0.90	0.72	2.64	2.57
	HZZ	0.96	0.80	2.61	2.52
E_{th} (eV)	HHZZ	0.37	0.47	1.88	1.85
	HHZ	0.61	0.45	1.55	1.77
	HZZ	0.64	0.51	1.48	1.74

The obtained charge localization energy values and defect level positions can be compared to the experimental electron trap thermal energy value of $W_t = 1.25$ eV and $W_{opt} = 2.5$ eV [22,23]. One can see that there is a good agreement between the calculation and the experiment for the optical trap energy and a satisfactory agreement for the thermal trap energy for neutral oxygen vacancy. These results show that the PATT model, based on neutral defects, is adequate to describe the transport.

The fact that the additional electron or hole is localized in the oxygen vacancy region is indicated by small peak width values (~ 0.1 eV) in the total density of states spectrum from the corresponding defective states in the bandgap. The fact of localization is also confirmed by the picture of the spatial distribution of the electron density difference with the up and down spin in a supercell of o-$Hf_{0.5}Zr_{0.5}O_2$ with an oxygen vacancy, as shown in Fig. 5. One can see that, when the excess charge is added to the defective structure, its localization takes place in the vacancy area and its first coordination sphere. The positive charge is distributed approximately uniformly between the nearest metal atoms to the vacancy. A negative charge is also distributed between the nearest neighbors, but only a pair of Hf-Zr atoms are bound. This feature is the subject of a further research.

4.4. Leakage current simulations

The leakage current depends exponentially on the voltage and can be described by the phonon-assisted tunneling between traps

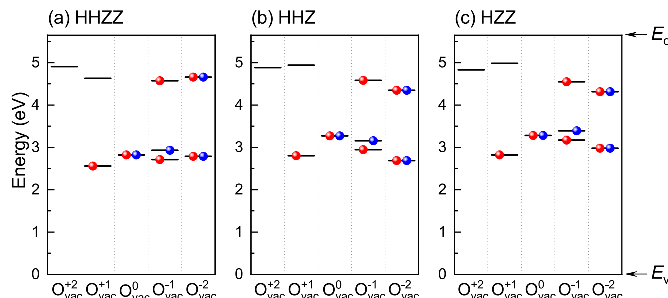

Fig. 4. The defect energy levels position in the bandgap of o-$Hf_{0.5}Zr_{0.5}O_2$ caused by the oxygen vacancies in coordination HHZZ (a), HHZ (b) and HZZ (c) in charge states $q = -2, -1, 0, +1, +2$.

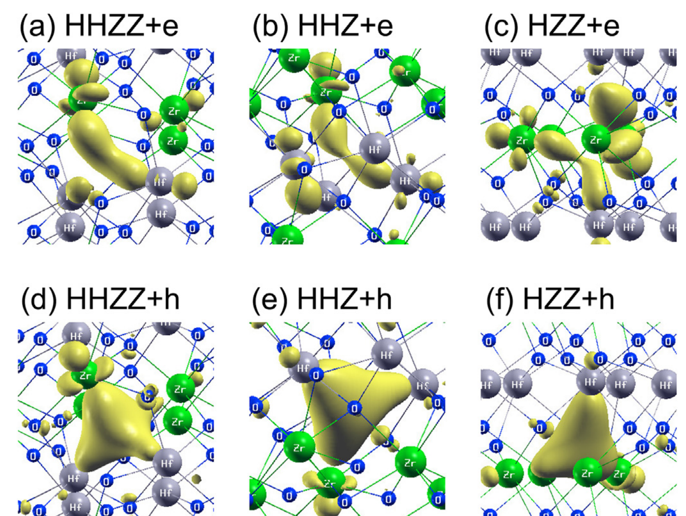

Fig. 5. Isosurfaces of equal magnitude of the charge density for the o-$Hf_{0.5}Zr_{0.5}O_2$ supercell with single-negatively charged (a), (b), (c) and positive d, (e), (f) oxygen vacancies in a different coordination.

model [27] and the approach described in section 3.1. A good qualitative and quantitative agreement between the experimental dependencies and calculated ones is reached with the following parameter values: thermal trap energy $W_t = 1.25$ eV, optical trap energy $W_{opt} = 2.5$ eV, effective mass $m^* = 0.37m_0$, part of filled traps $n_t/N = 0.5$. Here m_0 is the free electron mass. The obtained trap energies are related to the oxygen vacancy in $Hf_{0.5}Zr_{0.5}O_2$ [22,23,33]. Recently, it has been demonstrated that the well-known Frenkel model can describe the charge transport in $Hf_{0.5}Zr_{0.5}O_2$ using inadequate parameter values [22,23]. Indeed, the dynamic permittivity ε_∞ of the dielectric medium is included in the slope of the *I-V* curves on the $\log(I)$-$F^{1/2}$ plate. The slope decrease means that the ε_∞ value increases. This unphysical phenomenon proves that the Frenkel model cannot be used in the analysis of evolutionary leakage current-voltage dependencies.

The leakage current evolution, compared to MW during endurance tests, is shown in Fig. 6(a). The slope of the initial *I-V* curves on the semilog plot (Fig. 1(c)) corresponds to the largest distance between the nearest traps $a = 2.17$ nm (in case of a uniform distribution trap, a is the mean distance between traps, and the trap density is $N = 9.7 \times 10^{19}\text{cm}^{-3}$). After 10^4 set/reset cycles, the current increases spasmodically, and the $\log(I)$-V curves slope corresponds to $a = 2.15$ nm (and $N = 1 \times 10^{20}\text{cm}^{-3}$). During further cycles the current rises at a particular voltage on the test structure (Fig. 6(a)). After 10^8 cycles, the leakage current is described by the phonon-assisted tunneling between the traps with $a = 1.6$ nm ($N = 2.4 \times 10^{20}\text{cm}^{-3}$). The evolution of the mean distance between traps and the trap density during the endurance tests is shown in Fig. 6(b) by rounds and diamonds, respectively.

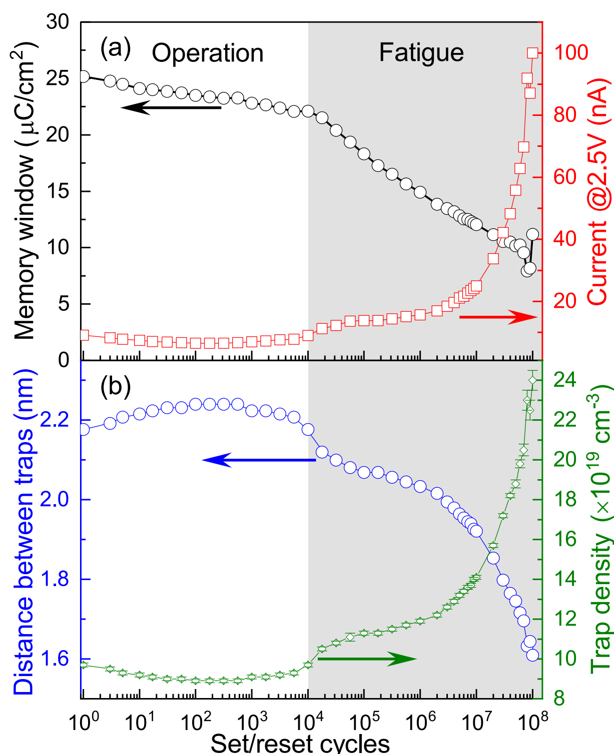

Fig. 6. (a) Evolution of the ferroelectric memory window (black rounds) with the leakage currents (red boxes) measured on the TiN/$Hf_{0.5}Zr_{0.5}O_2$ /TiN structure, (b) extracted mean distance between traps (blue rounds), as well as the defect concentration in case of uniform distribution (green diamonds). (For interpretation of the references to color in this figure legend, the reader is referred to the Web version of this article.)

4.5. Extended physical picture of field cycling degradation

Recently, it has been shown that the oxygen vacancies in hafnium oxide and zirconium oxide act as traps responsible for charge transport [28,34,35]. Moreover, the thermal and optical trap energies in HfO_2 and ZrO_2 are equal to $W_t = 1.25$ eV and $W_{opt} = 2.5$ eV, respectively. Taking into account the proximity of the oxygen vacancies electronic structure in HfO_2 [35–37] and ZrO_2 [38] (namely, the solid solution of these oxides is the studied $Hf_{0.5}Zr_{0.5}O_2$ films) and the equality of the trap energy parameters for HfO_2, ZrO_2 and $Hf_{0.5}Zr_{0.5}O_2$, it is not surprising that the oxygen vacancies act as the traps responsible for the charge transport in these dielectrics. Thus, it is very likely that the leakage currents in ferroelectric f-$Hf_{0.5}Zr_{0.5}O_2$ films correspond to intrinsic defects, namely oxygen vacancies.

According to the PATT model, the leakage current is limited by the region with the largest distance between traps. The distance between the traps, extracted from the leakage current simulations, in the operation mode (less than 10^4 cycles) increases from 2.17 nm to 2.24 nm. On the one hand, this can be interpreted as the annihilation of a small number of traps (oxygen vacancies). On the other hand, this can indicate that some defects are moving during the cycling, and the largest distance between the neighboring traps increases. Indeed, the occurrence of ferroelectric polarization in $Hf_{0.5}Zr_{0.5}O_2$ is due to the oxygen atom moving in the orthorhombic $Pbc2_1$ structure [39]. Thus, the ferroelectric switching can be accompanied by the oxygen atom-oxygen vacancy exchange between crystal cells, as well as by the annihilation of an interstitial-vacancy pair. No new oxygen vacancies are generated during the operation mode, as shown by the blue symbols in Fig. 7. A similar model of the oxygen vacancy moving before the fatigue was already proposed by Pešić et al. [15].

After 10^4 cycles, in the fatigue mode, the maximum distance between the traps decreased to 1.6 nm. This indicates that new oxygen vacancies are being generated, and SILC is getting dominant. Further, two possible events can occur. The first one is schematically depicted in Fig. 8. Yellow balls indicate the nearly-perfect-fluorite oxygen atom positions that would correspond to a zero ferroelectric polarization, blue balls indicate the oxygen positions

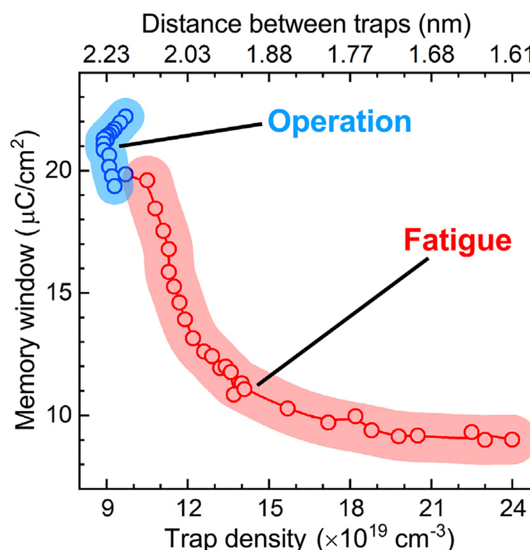

Fig. 7. Memory window dependencies on the extracted mean distance between the traps and trap density in $Hf_{0.5}Zr_{0.5}O_2$. The operation mode is highlighted in blue; the fatigue mode is colored in red. (For interpretation of the references to color in this figure legend, the reader is referred to the Web version of this article.)

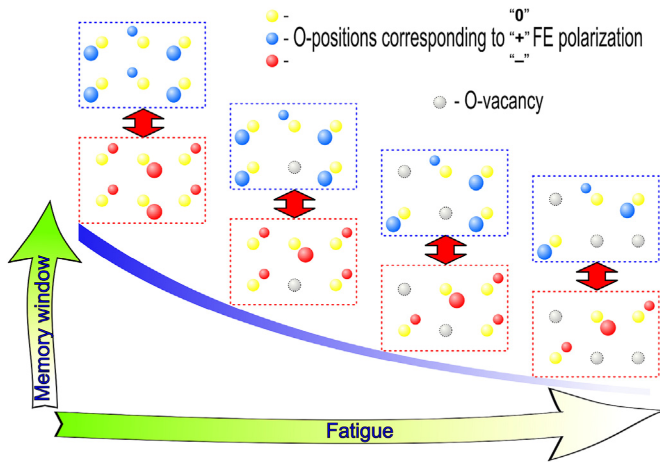

Fig. 8. A model of $Hf_{0.5}Zr_{0.5}O_2$ degradation (fatigue) due to the oxygen vacancy generation. The positions of oxygen atoms and vacancies, and their role in the ferroelectric response are described in the inset.

that would correspond to non-zero (e.g., positive) ferroelectric polarization, and red balls indicate the positions that would correspond to non-zero negative ferroelectric polarization. White spectre dashed-contoured balls symbolize oxygen vacancies. New oxygen vacancies generation decreases the number of oxygen atoms that can create a support for the ferroelectric polarization of the active medium by their movement (blue and red ball positions in Fig. 8). A new oxygen vacancy 'kills' the ferroelectricity in f-$Hf_{0.5}Zr_{0.5}O_2$, as shown in Fig. 8 by the spectre balls because the number of movable oxygen atoms is decreased. According to the main hypothesis of the ferroelectric switch mechanism in HfO_2-based films, the oxygen atom relocate in the $Pbc2_1$ lattice due to external electric field [39]. The periodical atom displacement in strong electric fields can lead to the heating and oxygen migration from the "correct" place in the lattice to an interstitial with a new Frenkel defect formation. Further electric fields cycling can lead to the Frenkel defect transformation into the Schottky-type defect, i.e. an oxygen vacancy generation. Recently, it has been found that the most probable positions of new defects (oxygen vacancies) are concentrated near an existing one [40]. This means that the more defects there are, the more new ones are generated. It is interesting to note that the total reduction of MW ($\approx 24/9$) is the same as the total increase of the trap density, as shown in Fig. 7. However, a more detailed quantitative analysis of the relationship between the amount of oxygen vacancies and ferroelectric polarization is still the subject of an ongoing research.

The second possible consequence of the increased oxygen vacancy density was suggested in Ref. [15] and it consists in pinning ferroelectric dipoles (or whole domains) by a trapped charge. This leads to a local shift of the coercive fields. Indeed, the oxygen vacancy in o-$Hf_{0.5}Zr_{0.5}O_2$ exhibits the amphoteric trapping nature and can localize both electrons and holes. Thus, the new traps generation leads to an increase of the localized charge in the dielectric bulk which can pin dipoles. Since both possible consequences of the increased vacancy concentration are probable, a combination of both effects is also very likely. The memory window reduction with the trap density increase (or distance between neighboring traps decrease) is indicated in Fig. 7 with the red symbols.

5. Conclusion

In conclusion, the nature of the traps responsible for the degradation mechanism of ferroelectric $Hf_{0.5}Zr_{0.5}O_2$ during the electric field cycling was studied. It has been proven that the oxygen vacancy in $Hf_{0.5}Zr_{0.5}O_2$ act as a charge localization center. Further, it was demonstrated that the leakage currents in thin ferroelectric $Hf_{0.5}Zr_{0.5}O_2$ films are described by the phonon-assisted tunneling between traps; the trap energy parameters are determined.

Using the phonon-assisted tunneling model developed by Nasyrov and Gritsenko, it is possible to determine the distance between traps and the trap density in $Hf_{0.5}Zr_{0.5}O_2$ from the slope of the current-voltage characteristics. Despite the fact that the trap density was extracted under the assumption of a uniform trap distribution over the whole film, the extracted values of the distance between traps mean the largest distance between the nearest traps in case of an arbitrary trap distribution. This leads to some distribution of a part of filled traps and does not contradict the dynamic charge trapping/detrapping due to a predominant traps generation, e.g. in the interface region.

Finally, it was demonstrated, that the oxygen vacancies are the traps responsible for the charge transport in $Hf_{0.5}Zr_{0.5}O_2$. Consequently, it should be possible to reduce the conductivity and, hence, leakage currents by decreasing the trap density. Possible changes in the technological process of $Hf_{0.5}Zr_{0.5}O_2$ film synthesis, could be, for example, the post-treatment annealing step in the oxygen atmosphere or using other precursors, e.g., oxygen O_2 [41] or ozone O_3 [42] as an oxidizing agent.

Acknowledgements

O.M.O. and G.Ya.K. are grateful to Evgeniy N. Morozov for their help in the endurance measurements. V.A.G. was supported by the Russian Science Foundation (Grant No. 14-19-00192). The simulation was performed using a computing cluster of the Rzhanov Institute of Semiconductor Physics SB RAS.

Appendix A. Supplementary data

Supplementary data to this article can be found online at https://doi.org/10.1016/j.actamat.2018.12.008.

References

[1] D. Bondurant, Ferroelectronic ram memory family for critical data storage, Ferroelectrics 112 (1990) 273–282, https://doi.org/10.1080/00150199008008233.
[2] C.-U. Pinnow, T. Mikolajick, Material aspects in emerging nonvolatile memories, J. Electrochem. Soc. 151 (2004) K13–K19, https://doi.org/10.1149/1.1740785.
[3] K. Maruyama, M. Kondo, S.K. Singh, H. Ishiwara, New ferroelectric material for embedded FRAM LSIs, Fujitsu Sci. Tech. J. 43 (4) (2007) 502–507.
[4] T.S. Böscke, J. Müller, D. Bräuhaus, U. Schröder, U. Böttger, Ferroelectricity in hafnium oxide thin films, Appl. Phys. Lett. 99 (2011) 102903, https://doi.org/10.1063/1.3634052.
[5] S. Mueller, J. Mueller, A. Singh, S. Riedel, J. Sundqvist, U. Schroeder, T. Mikolajick, Incipient ferroelectricity in Al-doped HfO_2 thin films, Adv. Funct. Mater. 22 (2012) 2412–2417, https://doi.org/10.1002/adfm.201103119.
[6] J. Müller, T.S. Böscke, U. Schröder, S. Mueller, D. Bräuhaus, U. Böttger, L. Frey, T. Mikolajick, Ferroelectricity in simple binary ZrO_2 and HfO_2, Nano Lett. 12 (2012) 4318–4323, https://doi.org/10.1021/nl302049k.
[7] Y. Matveyev, D. Negrov, A. Chernikova, Y. Lebedinskii, R. Kirtaev, S. Zarubin, E. Suvorova, A. Gloskovskii, A. Zenkevich, Effect of polarization reversal in ferroelectric TiN/$Hf_{0.5}Zr_{0.5}O_2$/TiN devices on electronic conditions at interfaces studied in operando by hard x-ray photoemission spectroscopy, ACS Appl. Mater. Interfaces 9 (49) (2017) 43370–43376, https://doi.org/10.1021/acsami.7b14369.
[8] A. Chernikova, M. Kozodaev, A. Markeev, D. Negrov, M. Spiridonov, S. Zarubin, O. Bak, P. Buragohain, H. Lu, E. Suvorova, A. Gruverman, A. Zenkevich, Ultrathin $Hf_{0.5}Zr_{0.5}O_2$ ferroelectric films on Si, ACS Appl. Mater. Interfaces 8 (11) (2016) 7232–7237, https://doi.org/10.1021/acsami.5b11653.
[9] M. Hyuk Park, H. Joon Kim, Y. Jin Kim, W. Lee, T. Moon, C. Seong Hwang, Evolution of phases and ferroelectric properties of thin $Hf_{0.5}Zr_{0.5}O_2$ films according to the thickness and annealing temperature, Appl. Phys. Lett. 102 (24) (2013) 242905, https://doi.org/10.1063/1.4811483.

[10] A. Chernikova, M. Kozodaev, A. Markeev, Y. Matveev, D. Negrov, O. Orlov, Confinement-free annealing induced ferroelectricity in $Hf_{0.5}Zr_{0.5}O_2$ thin films, Microelectron. Eng. 147 (2015) 15–18, https://doi.org/10.1016/j.mee.2015.04.024.

[11] F. Ambriz-Vargas, G. Kolhatkar, M. Broyer, A. Hadj-Youssef, R. Nouar, A. Sarkissian, R. Thomas, C. Gomez-Yáñez, M.A. Gauthier, A. Ruediger, A complementary metal oxide semiconductor process-compatible ferroelectric tunnel junction, ACS Appl. Mater. Interfaces 9 (15) (2017) 13262–13268, https://doi.org/10.1021/acsami.6b16173.

[12] S. Dunkel, M. Trentzsch, R. Richter, P. Moll, C. Fuchs, O. Gehring, M. Majer, S. Wittek, B. Muller, T. Melde, H. Mulaosmanovic, S. Slesazeck, S. Muller, J. Ocker, M. Noack, D.-A. Lohr, P. Polakowski, J. Muller, T. Mikolajick, J. Hontschel, B. Rice, J. Pellerin, S. Beyer, A FeFET based super-low-power ultra-fast embedded NVM technology for 22nm FDSOI and beyond, in: 2017 IEEE International Electron Devices Meeting (IEDM), IEEE, IEEE, 2017, https://doi.org/10.1109/iedm.2017.8268425, pp. 19.7.1–19.7.4.

[13] P. Polakowski, S. Riedel, W. Weinreich, M. Rudolf, J. Sundqvist, K. Seidel, J. Muller, Ferroelectric deep trench capacitors based on Al:HfO_2 for 3d nonvolatile memory applications, in: 2014 IEEE 6th International Memory Workshop (IMW), IEEE, IEEE, 2014, pp. 1–4, https://doi.org/10.1109/imw.2014.6849367.

[14] E. Yurchuk, J. Muller, J. Paul, T. Schlosser, D. Martin, R. Hoffmann, S. Mueller, S. Slesazeck, U. Schroeder, R. Boschke, R. van Bentum, T. Mikolajick, Impact of scaling on the performance of HfO_2-based ferroelectric field effect transistors, IEEE Trans. Electron. Dev. 61 (11) (2014) 3699–3706, https://doi.org/10.1109/ted.2014.2354833.

[15] M. Pešić, F.P.G. Fengler, L. Larcher, A. Padovani, T. Schenk, E.D. Grimley, X. Sang, J.M. LeBeau, S. Slesazeck, U. Schroeder, T. Mikolajick, Physical mechanisms behind the field-cycling behavior of HfO_2-based ferroelectric capacitors, Adv. Funct. Mater. 26 (2016) 4601–4612, https://doi.org/10.1002/adfm.201600590.

[16] F.P.G. Fengler, R. Nigon, P. Muralt, E.D. Grimley, X. Sang, V. Sessi, R. Hentschel, J.M. LeBeau, T. Mikolajick, U. Schroeder, Analysis of performance instabilities of hafnia-based ferroelectrics using modulus spectroscopy and thermally stimulated depolarization currents, Adv. Electron. Mater. 4 (3) (2018) 1700547, https://doi.org/10.1002/aelm.201700547.

[17] E.D. Grimley, T. Schenk, X. Sang, M. Pešić, U. Schroeder, T. Mikolajick, J.M. LeBeau, Structural changes underlying field-cycling phenomena in ferroelectric HfO_2 thin films, Adv. Electron. Mater. 2 (2016) 1600173, https://doi.org/10.1002/aelm.201600173.

[18] P. Giannozzi, S. Baroni, N. Bonini, M. Calandra, R. Car, C. Cavazzoni, D. Ceresoli, G.L. Chiarotti, M. Cococcioni, I. Dabo, A. Dal Corso, S. de Gironcoli, S. Fabris, G. Fratesi, R. Gebauer, U. Gerstmann, C. Gougoussis, A. Kokalj, M. Lazzeri, L. Martin-Samos, N. Marzari, F. Mauri, R. Mazzarello, S. Paolini, A. Pasquarello, L. Paulatto, C. Sbraccia, S. Scandolo, G. Sclauzero, A.P. Seitsonen, A. Smogunov, P. Umari, R.M. Wentzcovitch, QUANTUM ESPRESSO: a modular and open-source software project for quantum simulations of materials, J. Phys. Condens. Matter 21 (39) (2009) 395502, https://doi.org/10.1088/0953-8984/21/39/395502.

[19] P. Giannozzi, O. Andreussi, T. Brumme, O. Bunau, M.B. Nardelli, M. Calandra, R. Car, C. Cavazzoni, D. Ceresoli, M. Cococcioni, N. Colonna, I. Carnimeo, A.D. Corso, S. de Gironcoli, P. Delugas, R.A. DiStasio, A. Ferretti, A. Floris, G. Fratesi, G. Fugallo, R. Gebauer, U. Gerstmann, F. Giustino, T. Gorni, J. Jia, M. Kawamura, H.-Y. Ko, A. Kokalj, E. Küçükbenli, M. Lazzeri, M. Marsili, N. Marzari, F. Mauri, N.L. Nguyen, H.-V. Nguyen, A. O.-d. la Roza, L. Paulatto, S. Poncé, D. Rocca, R. Sabatini, B. Santra, M. Schlipf, A.P. Seitsonen, A. Smogunov, I. Timrov, T. Thonhauser, P. Umari, N. Vast, X. Wu, S. Baroni, Advanced capabilities for materials modelling with Quantum ESPRESSO, J. Phys. Condens. Matter 29 (46) (2017) 465901, https://doi.org/10.1088/1361-648x/aa8f79.

[20] Q. Zeng, A.R. Oganov, A.O. Lyakhov, C. Xie, X. Zhang, J. Zhang, Q. Zhu, B. Wei, I. Grigorenko, L. Zhang, L. Cheng, Evolutionary search for new high-k dielectric materials: methodology and applications to hafnia-based oxides, Acta Crystallogr. 70 (2014) 76–84, https://doi.org/10.1107/S2053229613027861.

[21] D. Muñoz Ramo, J.L. Gavartin, A.L. Shluger, G. Bersuker, Spectroscopic properties of oxygen vacancies in monoclinic HfO_2 calculated with periodic and embedded cluster density functional theory, Phys. Rev. B 75 (2007) 205336, https://doi.org/10.1103/PhysRevB.75.205336.

[22] D.R. Islamov, T.V. Perevalov, V.A. Gritsenko, C.H. Cheng, A. Chin, Charge transport in amorphous $Hf_{0.5}Zr_{0.5}O_2$, Appl. Phys. Lett. 106 (2015) 102906, https://doi.org/10.1063/1.4914900, arXiv:1501.02370.

[23] D.R. Islamov, A.G. Chernikova, M.G. Kozodaev, A.M. Markeev, T.V. Perevalov, V.A. Gritsenko, O.M. Orlov, Charge transport mechanism in thin films of amorphous and ferroelectric $Hf_{0.5}Zr_{0.5}O_2$, JETP Lett. 102 (2015) 544–547, https://doi.org/10.1134/S0021364015200047.

[24] S. Makram-Ebeid, M. Lannoo, Quantum model for phonon-assisted tunnel ionization of deep levels in a semiconductor, Phys. Rev. B 25 (1982) 6406–6424, https://doi.org/10.1103/PhysRevB.25.6406.

[25] K.A. Nasyrov, V.A. Gritsenko, Y.N. Novikov, E.-H. Lee, S.Y. Yoon, C.W. Kim, Two-bands charge transport in silicon nitride due to phonon-assisted trap ionization, J. Appl. Phys. 96 (8) (2004) 4293–4296, https://doi.org/10.1063/1.1790059.

[26] N. Novikov, V.A. Gritsenko, K.A. Nasyrov, Charge transport mechanism in amorphous alumina, Appl. Phys. Lett. 94 (2009) 222904, https://doi.org/10.1063/1.3151861.

[27] K.A. Nasyrov, V.A. Gritsenko, Charge transport in dielectrics via tunneling between traps, J. Appl. Phys. 109 (2011) 093705, https://doi.org/10.1063/1.3587452 [cited 2013.06.19].

[28] D.R. Islamov, V.A. Gritsenko, A. Chin, Charge transport in thin hafnium and zirconium oxide films, Optoelectron. Instrum. Data Process. 53 (2017) 184–189, https://doi.org/10.3103/S8756699017020121.

[29] D. Zhou, Y. Guan, M.M. Vopson, J. Xu, H. Liang, F. Cao, X. Dong, J. Mueller, T. Schenk, U. Schroeder, Electric field and temperature scaling of polarization reversal in silicon doped hafnium oxide ferroelectric thin films, Acta Mater. 99 (2015) 240–246, https://doi.org/10.1016/j.actamat.2015.07.035.

[30] R. Materlik, C. Künneth, T. Mikolajick, A. Kersch, The impact of charge compensated and uncompensated strontium defects on the stabilization of the ferroelectric phase in HfO_2, Appl. Phys. Lett. 111 (2017) 082902, https://doi.org/10.1063/1.4993110.

[31] F. Huang, X. Chen, X. Liang, J. Qin, Y. Zhang, T. Huang, Z. Wang, B. Peng, P. Zhou, H. Lu, L. Zhang, L. Deng, M. Liu, Q. Liu, H. Tian, L. Bi, Fatigue mechanism of yttrium-doped hafnium oxide ferroelectric thin films fabricated by pulsed laser deposition, Phys. Chem. Chem. Phys. 19 (2017) 3486–3497, https://doi.org/10.1039/c6cp07501k.

[32] S. Starschich, S. Menzel, U. Böttger, Pulse wake-up and breakdown investigation of ferroelectric yttrium doped HfO_2, J. Appl. Phys. 121 (2017) 154102, https://doi.org/10.1063/1.4981893.

[33] D.R. Islamov, A.G. Chernikova, M.G. Kozodaev, T.V. Perevalov, V.A. Gritsenko, O.M. Orlov, A.M. Markeev, Leakage currents mechanism in thin films of ferroelectric $Hf_{0.5}Zr_{0.5}O_2$, ECS Trans. 75 (2017) 123–129, https://doi.org/10.1149/07532.0123ecst.

[34] D.R. Islamov, V.A. Gritsenko, C.H. Cheng, A. Chin, Origin of traps and charge transport mechanism in hafnia, Appl. Phys. Lett. 105 (22) (2014) 222901, https://doi.org/10.1063/1.4903169, arXiv:1409.6887.

[35] V.A. Gritsenko, T.V. Perevalov, D.R. Islamov, Electronic properties of hafnium oxide: a contribution from defects and traps, Phys. Rep. 613 (2016) 1–20, https://doi.org/10.1016/j.physrep.2015.11.002.

[36] T.V. Perevalov, V.S. Aliev, V.A. Gritsenko, A.A. Saraev, V.V. Kaichev, E.V. Ivanova, M.V. Zamoryanskaya, The origin of 2.7 eV luminescence and 5.2 eV excitation band in hafnium oxide, Appl. Phys. Lett. 104 (2014) 071904, https://doi.org/10.1063/1.4865259.

[37] V.A. Gritsenko, D.R. Islamov, T.V. Perevalov, V.S. Aliev, A.P. Yelisseyev, E.E. Lomanova, V.A. Pustovarov, A. Chin, The oxygen vacancy in hafnia as a blue luminescence center and a trap of charge carriers, J. Phys. Chem. C 120 (2016) 19980–19986, https://doi.org/10.1021/acs.jpcc.6b05457.

[38] T.V. Perevalov, D.V. Gulyaev, V.S. Aliev, K.S. Zhuravlev, V.A. Gritsenko, A.P. Yelisseyev, The origin of 2.7 ev blue luminescence band in zirconium oxide, J. Appl. Phys. 116 (2014) 244109, https://doi.org/10.1063/1.4905105.

[39] S.V. Barabash, D. Pramanik, Y. Zhai, B. Magyari-Kope, Y. Nishi, Ferroelectric switching pathways and energetics in $(Hf,Zr)O_2$, ECS Trans. 75 (2017) 107–121, https://doi.org/10.1149/07532.0107ecst.

[40] A.A. Pil'nik, A.A. Chernov, T.V. Perevalov, D.R. Islamov, Simulations of correlative defect forming in hafnia, in: ECS Meeting Abstracts, Vol. MA2018-02, The Electrochemical Society, 2018, p. 691.

[41] D.R. Islamov, V.A. Gritsenko, M.S. Lebedev, Determination of trap density in hafnia films produced by two atomic layer deposition techniques, Microelectron. Eng. 178 (2017) 104–107, https://doi.org/10.1016/j.mee.2017.05.004.

[42] L. Wu, H.Y. Yu, Device performance and reliability improvement for MOSFETs with HfO_2 gate dielectrics fabricated using multideposition room-temperature multiannealing, IEEE Electron. Device Lett. 32 (9) (2011) 1173–1175, https://doi.org/10.1109/LED.2011.2158979.